Article

Not peer-reviewed version

A Microfluidic Method for Simultaneous Assessment of Blood Viscosity and Red Blood Cell Aggregation During Continuous Syringe Delivery

Yang Jun Kang *

Posted Date: 31 March 2026

doi: 10.20944/preprints202603.2297.v1

Keywords: blood viscosity; red blood cell aggregation; hemorheology; thermal-shock RBCs; sedimentation; microfluidics

 doi:10.20944/preprints202603.2297.v1

Article

A Microfluidic Method for Simultaneous Assessment of Blood Viscosity and Red Blood Cell Aggregation During Continuous Syringe Delivery

Yang Jun Kang

Department of Mechanical Engineering, Chosun University, 10, Chosundae 1-gil, Dong-gu, Gwangju 61452, Republic of Korea; yjkang2011@chosun.ac.kr; Tel.: +82-62-230-7052; Fax: +82-62-230-7055

Highlights

What are the main findings?

- A microfluidic-based method enabled simultaneous quantification of blood viscosity and RBC aggregation index under continuous blood flow from a driving syringe.
- Hemorheological properties were strongly affected by experimental factors and thermal shock, which suppressed RBC aggregation and sedimentation.

What are the implications of the main findings?

- The method allows reliable evaluation of blood properties under dynamic flow conditions, including syringe on–off operation.
- The method could be regarded as useful for assessing RBC dysfunction and abnormal hemorheological responses in microfluidic platforms.

Abstract

Accurate assessment of blood viscosity and red blood cell (RBC) aggregation under continuous flow is important for hemorheological analysis. However, simultaneous measurement remains challenging because both properties are influenced by flow conditions and RBC sedimentation. In this study, a microfluidic method is developed for the simultaneous measurement of blood viscosity and RBC aggregation index (AI) during continuous blood delivery from a driving syringe. The proposed device consists of a viscosity-sensing channel for viscosity measurement and aggregation-sensing channel for AI evaluation. The effects of flow rate, hematocrit, suspension medium, and syringe on-off operation are systematically investigated. Blood viscosity and AI are strongly affected by these factors and transient flow interruption enhances RBC sedimentation in the syringe, thereby altering hemorheological properties. The proposed method is further used to thermally shocked RBCs which reduce RBC aggregation and suppress RBC sedimentation when compared with control blood. At higher exposure temperatures and longer exposure times, blood viscosity and AI remain nearly constant over time, indicating minimal contribution of damaged RBCs to RBCs sedimentation. These results demonstrate that the proposed method enables reliable simultaneous evaluation of blood viscosity and RBC aggregation and could be regarded as useful for detecting functional alterations of RBCs under continuous-flow conditions.

Keywords: blood viscosity; red blood cell aggregation; hemorheology; thermal-shock RBCs; sedimentation; microfluidics

1. Introduction

Blood rheological properties are important clinical indicators because they directly affect flow resistance, microcirculatory perfusion, and oxygen delivery[1–4]. Whole-blood viscosity is a key

 doi:10.20944/preprints202603.2297.v1

determinant of vascular resistance, while RBC aggregation and deformability strongly influence blood flow behavior, particularly under low-shear and microvascular conditions[5]. Abnormal changes in these hemorheological properties are associated with impaired flow behavior in several disease states, and their measurement may therefore serve as a useful complementary approach for evaluating patient status[6], monitoring disease progression, and assessing therapeutic response[7–9].

Simultaneous assessment of blood viscosity and RBC aggregation is necessary to distinguish the biomechanical contributions of red blood cells and plasma proteins to hemorheological changes[10–12]. Blood viscosity reflects the bulk flow resistance of blood, whereas RBC aggregation is more directly associated with protein-mediated intercellular interactions and the surface or mechanical properties of red blood cells[13]. Accordingly, combined measurement of these two parameters enables more precise interpretation of whether the observed change arises predominantly from altered RBC biomechanics, modified plasma composition, or their combined effects.

Whereas conventional rheometers generally rely on larger sample volumes and bulk measurements, microfluidic chips enable physiologically relevant, low-volume, and highly integrated analysis of blood flow in microscale environments[14,15]. Several rheological properties, including, blood viscosity[16–26], RBC aggregation[27–31], RBC deformability[32–35], and so on are assessed in a microfluidic environment.

First, microfluidic devices estimated blood viscosity indirectly by analyzing hydrodynamic responses in microscale channels, including, pressure drop, blood flow-rate, and coflowing interface between two fluids. The most common working principle is pressure-drop viscometry, where blood is driven through a microchannel. Blood viscosity is then obtained using a Hagen–Poiseuille equation (i.e., pressure drop = fluidic resistance × flow rate)[15,36,37]. A second approach is coflowing or interface viscometry, where blood and reference fluid are simultaneously flowed in a single channel[20]. Blood viscosity is evaluated by assessing interface position between two streams. More recent methods determine blood viscosity by tracking blood flow during capillary filling[16,24] or pulsating motion in microchannels, which enables measurement of viscosity changes over time.

Second, RBC aggregation is typically measured by controlling the local shear condition and quantifying the optical signal generated by red blood cell clustering[38–40]. Because RBCs tend to form aggregates at low shears, most previous methods require temporary interruption of blood flow during measurement. At the stasis, RBC aggregates form and its aggregation index is calculated from timelapse image intensity[41], transmitted/backscattered light intensity[30,39,42], and electrical signal[43,44] within a specific region of interest. Some devices also use paired channel sections with different widths, so RBCs aggregate in a wide low-shear channel and are broken apart in a narrow high-shear channel[45]. The degree of aggregation is then estimated from the optical difference or intensity ratio between the aggregated and disaggregated states[46].

Although previous microfluidic methods have demonstrated on-chip measurement of blood viscosity and RBC aggregation[41,45,47], many of them still rely on interrupted flow, stationary-flow phases, or programmed stepwise flow control for assessing RBC aggregation effectively. For improving a real-time hemorheological monitoring, it needs to adopt simultaneous assessment of blood viscosity and RBC aggregation under continuous blood flow without intentional interruption of the blood stream. More recently, to resolve the issue, our group suggest new method for probing RBC aggregation in continuous fashion[48]. However, the method shows a limitation on simultaneous measurement of blood viscosity.

In this study, a new method is proposed to simultaneously measure blood viscosity and RBC aggregation under continuous blood flow without intentional flow interrupt. For this purpose, a microfluidic chip is newly designed to achieve the goal. Blood and a reference fluid (1× PBS) are delivered into the microfluidic chip with two syringe pumps. Based on our previous method[48], for inducing RBC aggregation under continuous-flow conditions, a bifurcation channel is branched from the main channel. The main channel provides high shear-rate region, whereas the bifurcation channel provides low shear-rate region that promotes RBC aggregation. The RBC aggregation index (AI) is

 doi:10.20944/preprints202603.2297.v1

then determined by analyzing image intensity values within branched channel and main channel. In addition, based on coflowing-stream method, blood viscosity is obtained from interfacial location between two fluids.

The present method has several advantages over previous approaches. It allows simultaneous quantification of blood viscosity and RBC aggregation in a single microfluidic system, reduces the need for separate measurements, and enables real-time evaluation under continuous syringe-driven flow. In addition, it can reflect dynamic effects such as RBC sedimentation and flow interruption, which are not easily captured by conventional methods. The method also provides a simple image-based platform for quantitative hemorheological analysis and is sufficiently sensitive to detect functional alterations in thermally damaged RBCs.

2. Materials and Methods

2.1. Microfluidic Chip and Experimental Setup

To measure blood viscosity and RBC aggregation under continuous blood flow, as shown in **Figure 1A**, an experimental setup was composed of a microfluidic chip, two syringe pumps, and image acquisition system.

As depicted in **Figure 1A-i**, a microfluidic chip was designed to have two inlets (a, b), main channel (mc), viscosity-sensing channel (vc), and aggregation-sensing channel (ac), and two outlets (a, b). When compared with our previous study[48], to measure blood viscosity, main channel was connected to the viscosity-sensing channel. Blood was loaded through main channel. Main channel (width = 1 mm, length = 14.5 mm) and aggregation-sensing channel had the same dimension and each channel consisted of three channels in series: a narrow-sized channel (width = 0.1 mm, length = 4.9 mm), a big-sized channel (width = 1 mm, length = 3 mm), and a narrow-sized channel (width = 0.1 mm, and length = 8.8 mm). All channels had a uniform depth of h = 0.05 mm.

A four-inch silicon master mold was fabricated using standard MEMS processes, including photolithography and deep reactive ion etching. PDMS (Sylgard 184, Dow Corning, Midland, MI, USA) was prepared by mixing the elastomer base and curing agent at a 10:1 ratio (w/w), degassing the mixture under vacuum for 1 h, and curing it at 65 °C for 2 h. After curing, the PDMS was peeled from the master, trimmed, and punched to form two inlets (outer diameter = 2 mm) and two outlets. It was then bonded to a glass substrate by oxygen plasma treatment (CUTE-MPR, Femto Science Co., South Korea) and heated at 120 °C for 10 min for strengthening PDMS–glass adhesion.

Each syringe was equipped with a 20-gauge needle and filled with blood (0.3 mL) or 1× PBS (1 mL). The needle was linked to the inlet port using polyethylene tubing (i.d. 0.25 mm, length 300 mm). Before the experiment, the microchannels were coated with 0.2% BSA for 10 min to prevent nonspecific protein adsorption, followed by washing with 1× PBS.

As shown in **Figure 1A-ii**, test blood and reference fluid were supplied into each inlet of a microfluidic chip. Herein, 1× PBS was selected as reference fluid. The corresponding flow rate of each fluid was denoted as Q_b (test blood) and Q_r (reference fluid), respectively. During blood delivery, RBC sedimentation proceeded continuously depending on RBC mechanical properties[49], hematocrit[50,51], and blood medium[29,52,53]. Continuous RBC sedimentation contributed to changing hematocrit of test blood flowing in the microfluidic chip[54,55]. The right-side panel represented timelapse snapshot for RBC sedimentation within an elapse of period.

 doi:10.20944/preprints202603.2297.v1

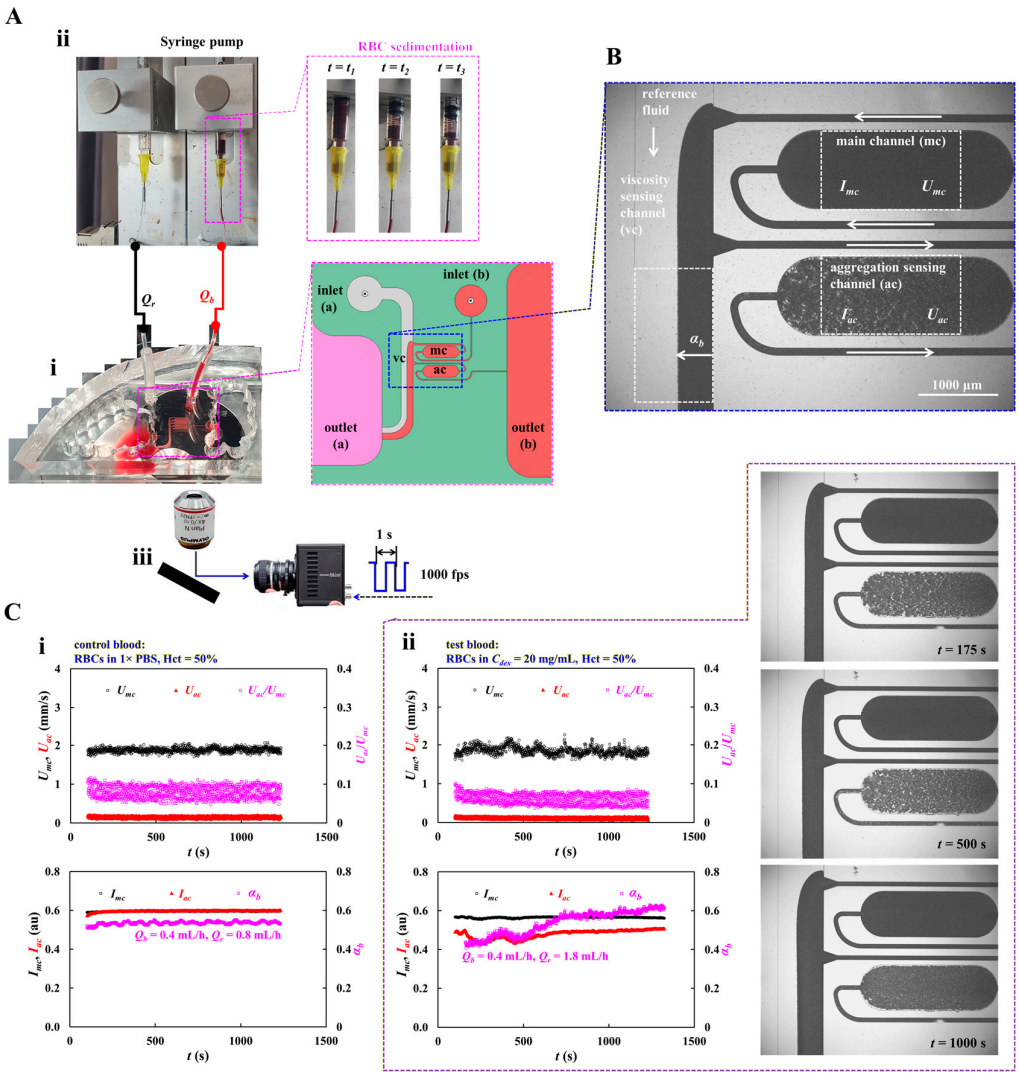

Figure 1. A microfluidic platform proposed for assessing blood viscosity and RBC aggregation in continuous blood flow. **(A)** Experimental setup, including, a microfluidic device, two syringe pumps, and image acquisition system. **(i)** Microfluidic device was designed to have two inlets (a, b), main channel (mc), viscosity-sensing channel (vc), and aggregation-sensing channel (ac), and two outlets (a, b). **(ii)** Two syringe pumps for supplying blood and reference fluid (1× PBS). Flow rate of each fluid was set to Q_b (blood) and Q_r (1× PBS). Right side panel showed RBC sedimentation in a driving syringe during blood delivery. **(iii)** Image acquisition system, including, microscopy (4× objective lens, NA = 0.1), high-speed camera (1000 fps), and function generator (triggering period: 1 s). **(B)** Quantification of blood velocity (U_{mc}, U_{ac}), imaging intensity (I_{mc}, I_{ac}), and interface (α_b) in the microfluidic channels. Herein, ROI of main channel (mc) and aggregation-sensing channel (ac) was selected within big-sized channel. The ROI of viscosity-sensing channel (vc) was positioned slightly below the junction point of aggregation channel. The ROI of each channel was set to 1.8 mm^2. **(C)** Preliminary demonstration of the proposed method. Herein, hematocrit of two bloods (control blood, and test blood) were adjusted to Hct = 50% by suspending normal RBCs into 1× PBS and dextran solution (20 mg/mL), respectively. **(i)** Timelapse blood velocity (U_{mc}, U_{ac}), image intensity (I_{mc}, I_{ac}), and interface (α_b) of control blood. Herein, flow rate of each fluid was set to Q_b = 0.4 mL/h and Q_r = 0.8 mL/h, respectively. **(ii)** Timelapse blood velocity (U_{mc}, U_{ac}), image intensity (I_{mc}, I_{ac}), and interface (α_b) of test blood. Herein, flow rate of each fluid was set to Q_b = 0.4 mL/h and Q_r = 1.8 mL/h, respectively. Right-side panel depicted microscopic images captured at t = 175, 500, and 1000 s.

 doi:10.20944/preprints202603.2297.v1

The device was observed under an inverted microscope (IX81, Olympus, Tokyo, Japan) fitted with a 4× objective (NA = 0.10). Flow images were captured at 1000 frames/s using a high-speed camera with an external trigger every 1 s, and all tests were carried out at room temperature (25 °C).

2.2. Quantification of Blood Velocity, Image Intensity, and Interface

In this study, blood velocity in the main and aggregation channels was measured simultaneously to determine the flow rate entering the viscosity-sensing channel from the syringe. RBC aggregation index was obtained from image intensity in the main and aggregation-sensing channels. Furthermore, blood viscosity was estimated from the interface in the viscosity-sensing channel.

First, for quantifying average blood velocity in the main and aggregation-sensing channels, a specific ROI (1.8 mm²) was selected in the largest channel region. Timelapse velocity fields were analyzed using PIVlab (Version: 3.12)[56] with interrogation window of 67 × 67 μm² and 50% overlap, and the resulting vectors were filtered using local median and standard-deviation methods. Since the DOC was estimated to be greater than 300 μm and exceeded the channel depth of 50 μm [57], the measured velocities were assumed to represent depth-averaged velocity. Average velocities over each ROI were then defined as $\langle U_{mc} \rangle$ and $\langle U_{ac} \rangle$, and were used to calculate $Q_{ac} = (\langle U_{ac} \rangle / \langle U_{mc} \rangle) \times Q_b$ and $Q_{vc} = Q_b - Q_{ac}$.

Second, to quantify RBC aggregation, each image was subtracted from the initial background image and analyzed using MATLAB (Version 2025b, MathWorks, Natick, MA, USA). A ROI (1.8 mm²) was defined in the largest region of the main and aggregation-sensing channels, and the mean grayscale intensities were obtained as I_{mc} and I_{ac}, respectively. The same process was applied to all image sets.

Third, to quantify the interface in the viscosity-sensing channel, grayscale images were binarized using Otsu's method. A specific ROI (1.8 mm²) was selected in the straight coflowing downstream of the aggregation-sensing channel junction. The average blood-filled width within the ROI was defined as w_b, and the normalized interface was expressed as $\alpha_b = w_b/w$, where channel width was denoted as w = 1 mm.

As a preliminary demonstration, control blood and test blood were prepared by suspending normal RBCs into 1× PBS and dextran solution (20 mg/mL), respectively. Hematocrit of each blood was set to Hct = 50%. Herein, blood flow-rate set to Q_b = 0.4 mL/h. Based on shear-rate formula of low-asepct rectangular channel (i.e., $\dot{\gamma} = \frac{6\,Q}{w\,h^2}$) [37], the corresponding shear rate of wide-width channel and narrow-width channel was estimated as $\dot{\gamma} = 266.7\ s^{-1}$ (wide-width channel) and $\dot{\gamma} = 2666.7\ s^{-1}$ (narrow-width channel), respectively. As shown in **Figure 1C-i**, with respect to control blood, timelapse blood velocity (U_{mc}, U_{ac}), image intensity (I_{mc}, I_{ac}), and interface (α_b) were obtained. Herein, to relocate inteface near channel width, flow rate of 1× PBS was set to Q_r = 0.8 mL/h. All parameters remained constant over period. On the other hand, as depicted in **Figure 1C-ii**, with regard to test blood, timelapse blood velocity (U_{mc}, U_{ac}), image intensity (I_{mc}, I_{ac}), and interface (α_b) were obtained. Initially, to relocated interface near channel width, flow rate of 1× PBS was set to Q_r = 1.8 mL/h. Right-side panel depicted microscopic images captured at t = 175, 500, and 1000 s. When compared with main channel and viscosity-sending channel, RBC aggregation was clearly observed within aggregation-sensing channel. U_{mc}, U_{ac}, and U_{ac}/U_{mc} did not show substantial variations over time, where blood flow-rate maintained constant. However, as shown in **Figure 1A-ii**, dextran solution (20 mg/mL) caused RBCs sedimentation in a driving syringe during blood delivery. Accordingly, a clear difference in image intensity (i.e., $\Delta I = I_{mc} - I_{ac}$) was observed, which gradually decreased over time. The interface increased progressively. From the results, image intensity and interface could be used to detect substantial blood-to-blood difference.

2.3. Blood Sample Preparation

Packed RBCs were provided by the Gwangju–Chonnam Blood Bank (Gwangju, South Korea) and kept refrigerated before sample preparation. Normal RBCs were isolated according to an

 doi:10.20944/preprints202603.2297.v1

established washing procedure [58] by sequential removal of blood medium and buffy coat, and the procedure was repeated twice.

Three sets of test blood were prepared. First, hematocrit-dependent effects were examined using normal RBCs suspended into dextran solution (20 mg/mL) at Hct = 30–60%. Second, medium-dependent effects were evaluated by suspending normal RBCs into dextran solutions of 5–20 mg/mL in 1× PBS at a fixed Hct of 50%. Third, thermally treated RBCs were prepared by incubating normal RBCs at 40 ~ 50 °C for up to 180 min, followed by washing and resuspension in dextran solution (20 mg/mL) at Hct = 50%.

3. Results and Discussion

3.1. Quantitative Evaluation of the Proposed Method

In this section, as shown in **Figure 1C**, timelapse blood velocities, image intensities, and interface were used to quantify blood viscosity and aggregation index.

First, as shown in **Figure 2A**, a coflowing streams method was used to obtain blood viscosity[59,60]. As shown in left-side panel, using two syringe pumps, flow rate of test blood and 1× PBS was set to Q_r and Q_b, respectively. A portion of the syringe-delivered blood entered the aggregation-sensing channel at a flow rate of Q_{ac}, while the remaining blood flowed into the viscosity-sensing channel at $Q_b - Q_{ac}$. In the viscosity-sensing channel, the test blood and 1× PBS flowed in parallel at $Q_b - Q_{ac}$ and Q_r, respectively. To derive viscosity formula, as shown in right-side panel, a simple fluidic circuit model of coflowing stream method was constructed using a discrete fluid element, including, flow rate (Qr, Q_b - Q_{ac}), and fluidic resistance (R_r, R_b). The R_r and R_b represent equivalent fluidic resistance of 1× PBS stream and test blood stream, respectively. Considering that both streams had the same pressure drop (i.e., $\Delta P_r = \Delta P_b$), blood viscosity formula was derived as $\mu_b = \mu_r \left(\frac{\alpha_b}{1-\alpha_b}\right)\left(\frac{Q_r}{Q_b - Q_{ac}}\right) C_f(\alpha_b)$. Herein, the $C_f(\alpha_b)$ denoted correction factor which depended on channel dimension and interfacial location[61]. According to the previous study[60], with respect to microfluidic channel (i.e., width = 1 mm, and depth = 0.05 mm), the correction factor was given as $C_f(\alpha_b) = -12.038\,\alpha_b^4 + 26.171\,\alpha_b^3 - 20.770\,\alpha_b^2 + 77.156\,\alpha_b + 0.014$ ($R^2 = 0.970$). In addition, shear rate of test blood-stream in the viscosity-sensing channel was derived as $\dot{\gamma} = \frac{6(Q_b - Q_{ac})}{\alpha_b w\, h^2}$.

Second, blood velocity had to be calibrated to obtain flow rate. Because micro-PIV measurements were affected by hematocrit[62], velocity alone was insufficient for accurate flow-rate estimation. As the test blood was delivered at a constant flow rate, the measured velocity could be used to determine flow rate after calibration. As shown in left-side panel of **Figure 2B**, timelapse U_{mc} and U_{ac} of test blood were plotted for explaining calibration procedure. The steady plateau value of U_{mc} was obtained as $\langle U_{mc} \rangle$ = 1.85 mm/s. The corresponding flow rate of each velocity was calibrated as $Q_{mc} = U_{mc}/\langle U_{mc} \rangle \times Q_b$, and $Q_{ac} = U_{ac}/\langle U_{mc} \rangle \times Q_b$, respectively. Right-side panel of **Figure 2B** showed timelapse Q_{mc} and Q_{ac}. As a result, flow rate of Q_{mc} and Q_{ac} was obtained as Q_{mc} = 0.40 ± 0.02 mL/h (n = 1224) and Q_{ac} = 0.02 ± 0.01 mL/h (n = 1224), respectively. The results indicated that only 5% of the test blood entered the aggregation channel, whereas the remaining 95% flowed into the viscosity-sensing channel.

Third, based on our previous method[48], RBC aggregation index (AI) was calculated using timelapse I_{mc} and I_{ac}. As shown in **Figure 1C**, with regard to control blood, I_{mc} and I_{ac} were overlapped over time. However, when 1× PBS was replaced by dextran solution (20 mg/mL), the I_{ac} was decreased substantially when compared with I_{mc}. That is, RBC aggregation contributed to decreasing I_{ac} considerably. The ΔI (i.e., $\Delta I = I_{mc} - I_{ac}$) represented the strength of RBC aggregation appropriately[48]. As shown in **Figure 3C**, by normalizing ΔI with I_{mc}, the RBC aggregation index was expressed as AI = $(I_{mc} - I_{ac})/I_{mc}$. This simple equation enabled continuous time-lapse measurement of AI without stopping the blood flow.

 doi:10.20944/preprints202603.2297.v1

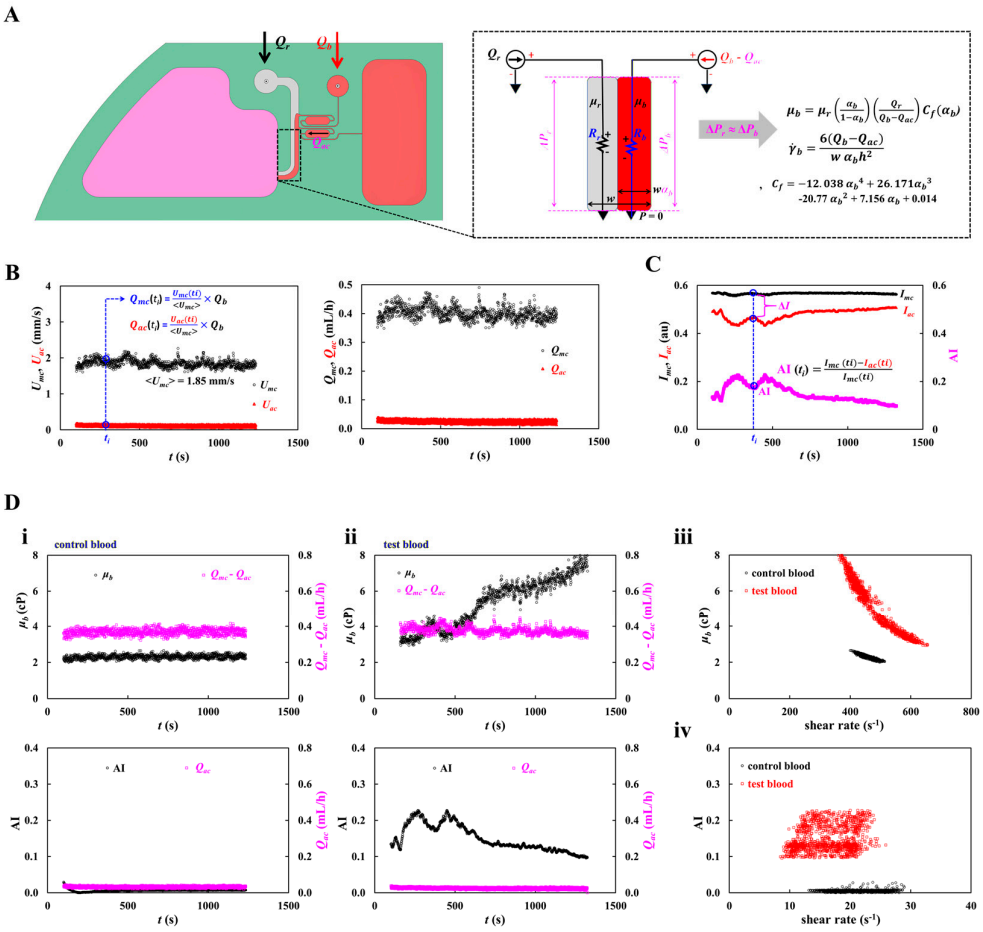

Figure 2. Quantitative comparison between control blood and test blood using blood viscosity and aggregation index in continuous blood flow. **(A)** Blood viscosity measurement using coflowing streams method. Left-side panel represented flow rate of each stream (blood stream: Q_b – Q_{ac}, and reference stream: Q_r) in the ROI of viscosity-sensing channel. Right-side panel showed viscosity formula using coflowing streams method. **(B)** Calibration of Q_{mc} and Q_{ac} using steady plateau value of U_{mc}. Left-side panel represented timelapse U_{mc} and U_{ac}. Herein, the steady plateau value of U_{mc} was obtained as $\langle U_{mc} \rangle = 1.85$ mm/s. The corresponding flow rate of each velocity was calibrated as $Q_{mc} = U_{mc}/\langle U_{mc} \rangle \times Q_b$, and $Q_{ac} = U_{ac}/\langle U_{mc} \rangle \times Q_b$, respectively. Right-side panel showed timelapse Q_{mc} and Q_{ac}. **(C)** Aggregation index (AI) calculation using I_{mc} and I_{ac}. As the ΔI (i.e., ΔI=Imc-Iac) was proportional to RBC aggregation, the AI as normalized form was defined as $AI = (I_{mc} - I_{ac})/I_{mc}$. **(D)** Quantitative comparison between control blood and test blood. **(i)** Timelapse μ_b and AI of control blood. **(ii)** Timelapse μ_b and AI of test blood. **(iii)** Comparison of blood viscosity between two bloods. **(iv)** Comparison of AI between two bloods.

At last, based on the calculation procedures for flow rate, blood viscosity, and the RBC aggregation index, as shown in **Figure 2D**, control and test blood samples were quantitatively compared using viscosity and the RBC aggregation index. As shown in **Figure 4D-i**, with regard to control blood, the upper panel exhibited timelapse μ_b and Q_{mc} - Q_{ac}. The lower panel showed timelapse AI and Q_{ac}. Accordingly, the μ_b and was obtained as $\mu_b = 2.31 \pm 0.11$ cP. Herein, number of data was denoted as $n = 1134$. The Q_{mc} - Q_{ac} was acquired as Q_{mc} - $Q_{ac} = 0.37 \pm 0.02$ mL/h. In addition, AI and Q_{ac} were obtained as AI = 0.01 ± 0.003 and $Q_{ac} = 0.03 \pm 0.01$ mL/h. As depicted in **Figure 2D-ii**, timelapse μ_b and AI of test blood were obtained. The upper panel exhibited timelapse μ_b and Q_{mc} - Q_{ac}. During blood delivery, blood viscosity increased from $\mu_b = 2.93$ cP to $\mu_b = 8.15$ cP significantly. Herein, number of data was denoted as $n = 1165$. The Q_{mc} - Q_{ac} maintained constant as Q_{mc} - $Q_{ac} = 0.38 \pm 0.02$ mL/h. Accordingly, RBC sedimentation in a driving syringe proceeded over time[54], which contributed to

 doi:10.20944/preprints202603.2297.v1

increasing blood viscosity over time. However, the flow-rate of Q_{mc} and Q_{ac} maintained constant because flow rate of test blood set to Q_b = 0.4 mL/h. The lower panel showed the timelapse variations of AI and Q_{ac}. Initially, AI was 0.13 and gradually increased to 0.23. It then fluctuated between 0.23 and 0.17 before eventually decreasing from 0.23 to 0.10 over time. In contrast, Q_{ac} remained nearly constant at 0.025 ± 0.006 mL/h. These results indicated that the RBC aggregation index changed continuously with the progression of RBC sedimentation in the driving syringe. Shear rate in viscosity-sensing channel was estimated using timelapse α_b and (Q_{mc} – Q_{ac}). As shown in **Figure 2D-iii**, blood viscosity (μ_b) of each blood was plotted as a function of shear rate ($\dot{\gamma}$). The viscosity of test blood was much larger than that of control blood. As shown in **Figure 1C**, as RBC sedimentation of test blood was proceeded over time, interface increased substantially which resulted in decreasing shear rate. **Figure 2D-iv** exhibited variations of AI between two bloods with respect to shear rate. Compared with the control blood, the test blood showed a higher AI, while its shear rate was slightly reduced as a result of Q_{ac}.

The quantitative comparison demonstrated that the proposed method was effective for discriminating between control and test blood during continuous flow from a driving syringe.

3.2. Contribution of Blood Flow-Rate, Hematocrit, and Suspending Medium

According to the previous studies, blood viscosity and AI were significantly influenced by flow condition, hematocrit, and suspending medium [5,10,63–67]. In this section, the proposed method was used to evaluate the effects of several factors on both properties under a constant blood flow rate, with blood continuously delivered from a driving syringe into the microfluidic chip.

First, as shown in **Figure 3A**, blood viscosity (μ_b) and RBC aggregation index (AI) were obtained with respect to Q_b = 0.2 ~ 0.8 mL/h. Herein, test blood (Hct = 50%) was prepared by suspending normal RBCs into dextran solution (20 mg/mL). **Figure 3A-i** showed timelapse Q_{mc} and Q_{ac} with respect to Q_b. The corresponding Q_{mc} of each Q_b were obtained as Q_{mc} = 0.2 ± 0.01 mL/h (n = 2042) for Q_b = 0.2 mL/h, Q_{mc} = 0.4 ± 0.03 mL/h (n = 1133) for Q_b = 0.4 mL/h), Q_{mc} = 0.6 ± 0.04 mL/h (n = 1101) for Q_b = 0.6 mL/h), and Q_{mc} = 0.8 ± 0.05 mL/h (n = 675) for Q_b = 0.8 mL/h. Additionally, the corresponding Q_{ac} of each Q_b were obtained as Q_{ac} = 0.01 ± 0.01 mL/h for Q_b = 0.2 mL/h, Q_{ac} = 0.03 ± 0.01 mL/h for Q_b = 0.4 mL/h), Q_{ac} = 0.04 ± 0.01 mL/h for Q_b = 0.6 mL/h), and Q_{ac} = 0.05 ± 0.01 mL/h for Q_b = 0.8 mL/h. The results showed that both flow rates (Q_{mc}, Q_{ac}) remained stable over time and were accurately adjusted in proportion to Q_b. **Figure 3A-ii** showed timelapse μ_b and AI with respect to Q_b. The upper panel exhibited time-dependent μ_b with respect to Q_b. For the given Q_b range, the shear rate in the main channel was estimated as $\dot{\gamma}$ = 133.3 ~ 533.3 s^{-1}. Initially, μ_b was almost independent of Q_b. As time elapsed, its fluctuation increased significantly at lower Q_b compared with higher Q_b, owing to RBC sedimentation in the driving syringe rather than shear-thinning effect. The lower panel depicted timelapse AI with respect to Q_b. As expected, lower Q_b had higher value of AI when compared with higher Q_b. The AI tended to decrease significantly over time. As RBC sedimentation proceeded over time, hematocrit of blood supplied into a microfluidic chip increased over time. For the reason, it was inferred that RBCs sedimentation in a driving syringe contributed to increasing blood viscosity and AI continuously. As shown in **Figure 3A-iii**, variations of μ_b and AI were plotted as a function of shear rate ($\dot{\gamma}$). Lower Q_b resulted in higher μ_b and substantially higher AI compared with higher Q_b. Given the strong influence of Q_b on both parameters, Q_b was fixed at 0.4 mL/h for the following experiments.

Second, as represented in **Figure 3B**, variations of blood viscosity (μ_b) and RBC aggregation index (AI) were obtained as a function of hematocrit. To probe impact of hematocrit on both properties, hematocrit of test blood was adjusted to Hct = 30% ~ 60% by adding normal RBCs into dextran (20 mg/mL). Flow rate of blood was fixed at Q_b = 0.4 mL/h. As shown in **Figure 3B-i**, timelapse Q_{mc} and Q_{ac} were obtained with respect to Hct. The Q_{mc} remained nearly constant regardless of Q_b, whereas Q_{ac} tended to increase with respect to Hct. This increase in hematocrit attributed to elevated junction pressure between the viscosity-sensing and aggregation-sensing channels, which resulted in increasing Q_{ac} substantially. As shown in **Figure 3B-ii**, timelapse μ_b and AI were obtained with respect to Hct. In the upper panel, the μ_b initially increased with respect to hematocrit and rose

 doi:10.20944/preprints202603.2297.v1

further over time. However, no marked difference was observed among Hct conditions. In the lower panel, the AI decreased significantly with increasing Hct and decreased continuously over time. As shown in **Figure 3B-iii**, variations of μ_b and AI were plotted as a function of shear rate ($\dot{\gamma}$) with respect to Hct. Although Q_b was kept constant, higher viscosity increased blood-filled width, which reduced shear rate in viscosity-sensing channel. That is, higher viscosity caused to lower shear rate. The results showed that hematocrit contributed to increasing μ_b significantly, whereas the AI decreased markedly with respect to Hct. However, the AI did not exhibit substantial variations with respect to shear rate. Therefore, hematocrit of test blood was fixed at Hct = 50% in subsequent experiments.

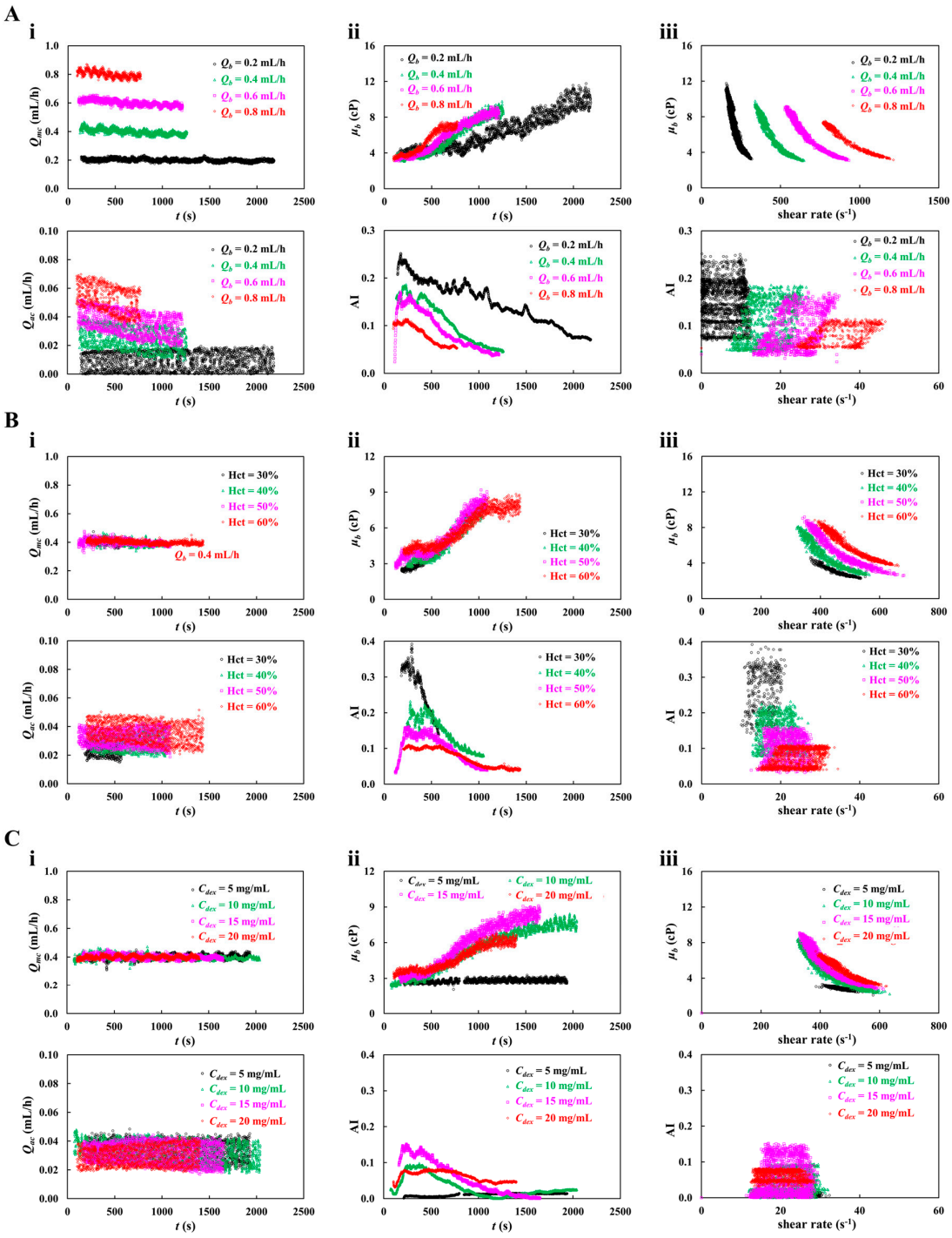

 doi:10.20944/preprints202603.2297.v1

Figure 3. Contribution of flow rate, hematocrit, and blood medium (dextran solution) to blood viscosity and RBC aggregation. **(A)** The effect of blood flow-rate on blood viscosity (μ_b) and RBC aggregation index (AI). Herein, test blood (Hct = 50%) was prepared by suspending normal RBCs into dextran solution (20 mg/mL). **(i)** Timelapse Q_{mc} and Q_{ac} with respect to Q_b = 0.2 ~ 0.8 mL/h. **(ii)** Timelapse μ_b and AI with respect to Q_b. **(iii)** Variations of μ_b and AI as a function of shear rate ($\dot{\gamma}$) with respect to Q_b. **(B)** Contribution of hematocrit (Hct) to blood viscosity (μ_b) and RBC aggregation index (AI). Herein, hematocrit of test blood was adjusted to Hct = 30% ~ 50% by adding normal RBCs into dextran solution (20 mg/mL). Flow rate of blood was fixed at Q_b = 0.4 mL/h. **(i)** Timelapse Q_{mc} and Q_{ac} with respect to Hct. **(ii)** Timelapse μ_b and AI with respect to Hct. **(iii)** Variations of μ_b and AI as a function of shear rate ($\dot{\gamma}$) with respect to Hct. **(C)** Contribution of dextran solution to blood viscosity and RBC aggregation index. Herein, hematocrit and flow-rate of blood were set to Hct = 50% and Q_b = 0.4 mL/h, respectively. **(i)** Timelapse Q_{mc} and Q_{ac} with respect to C_{dex} = 5 ~ 20 mg/mL. **(ii)** Timelapse μ_b and AI with respect to C_{dex}. **(iii)** Variations of μ_b and AI as a function of shear rate ($\dot{\gamma}$) with respect to C_{dex}. .

Third, to investigate impact of suspending medium on both properties, several different concentrations of dextran solution (C_{dex} = 5 ~ 20 mg/mL) were used as blood medium. Herein, test blood (Hct = 50%) was prepared by adding normal RBCs into a specific dextran solution. Blood flow-rate was set to Q_b = 0.4 mL/h. As shown in **Figure 3C-i**, timelapse Q_{mc} and Q_{ac} were obtained with respect to C_{dex} = 5 ~ 20 mg/mL. According to the results, Q_{mc} remained constant with respect to C_{dex}. Additionally, dextran solution did not contribute to varying Q_{ac} substantially. **Figure 3C-ii** exhibited timelapse μ_b and AI with respect to C_{dex}. With the exception of C_{dex} = 5 mg/mL, dextran contributed to a time-dependent increase in blood viscosity. Blood suspended in C_{dex} = 15 mg/mL exhibited the highest μ_b and AI, while AI declined markedly over time. As shown in **Figure 3C-iii**, variations of μ_b and AI were plotted as a function of shear rate ($\dot{\gamma}$) with respect to C_{dex}. The results showed that μ_b changed markedly with shear rate. With the exception of C_{dex} = 5 mg/mL, the shear-dependent variation in μ_b was comparable among C_{dex} = 10 ~ 20 mg/mL.
However, AI showed no substantial dependence on shear rate and exhibited large fluctuations, with the highest value observed at C_{dex} = 15 mg/mL.

The experimental investigation demonstrated that syringe flow rate, hematocrit, and suspending medium had significant effects on blood viscosity and RBC aggregation index. Accordingly, to obtain consistent measurements, these three factors were strictly controlled in the following experiments.

3.3. Evaluation of No-Delivery Waiting Time Under RBCs Sedimentation

In Section 3.2, RBC sedimentation during continuous blood delivery with a syringe pump strongly affected blood viscosity and the RBC aggregation index. In this section, no-delivery waiting time (T_w), which was defined as the elapsed time after stopping the syringe pump, was introduced as a new factor to accelerate RBC sedimentation. Test blood (Hct = 50%) was prepared by suspending normal RBCs in dextran solution (20 mg/mL). The corresponding flow rate of blood and 1× PBS was set to Q_b = 0.4 mL/h and Q_r = 1.8 mL/h, respectively.

First, as shown in **Figure 4A**, impact of no-delivery waiting time (T_w) on blood viscosity (μ_b) and RBC aggregation index (AI) were quantitatively evaluated. As depicted in **Figure 4A-i**, to visualize RBC sedimentation in the driving syringe, snapshots were taken at specific no-delivery waiting times (T_w = 0 ~ 40 min) under no blood flow condition (Q_b = 0). RBC sedimentation proceeded continuously and was clearly observed after an elapse of 20 min. **Figure 4A-ii** exhibited timelapse α_b, I_{mc}, and I_{ac} with respect to T_w = 0, 30 min. At T_w = 30 min, the rise time of α_b became shorter, but its plateau value remained essentially unchanged. Additionally, the image intensity difference ($\Delta I = I_{mc} - I_{ac}$) was reduced. The results indicated that no-delivery waiting time had a strong impact on α_b and ΔI. To find out contribution of T_w to interface and image intensity, as shown in **Figure 4A-iii**, timelapse α_b, I_{mc}, and I_{ac} were acquired with respect to T_w = 0 ~ 40 min. In the left panel, the time-course of α_b exhibited a similar increasing trend for T_w = 10 ~ 40 min, except for T_w = 0. In an initial perid of blood delivery, α_b showed large fluctuations. During the no-delivery waiting period, RBC sedimentation

 doi:10.20944/preprints202603.2297.v1

occurred in the fluidic path, including the inlet tubing and syringe needle, resulting in a nonuniform hematocrit distribution. At Qb = 0.4 mL/h, the transit time from the needle tip to the inlet port was estimated to be 132 s. Therefore, after flow resumed, sufficient transit time and shear exposure were required to disperse RBC aggregates and restore a homogeneous RBC suspension before entry into the microfluidic chip[42,45,68]. The middle panel shows that I_{mc} decreased significantly after T_w = 10 min, and then remained nearly independent of T_w. In the right panel, I_{ac} increased slightly after T_w = 10 min. **Figure 4A-iv** showed timelapse μ_b and AI with respect to T_w. Compared with T_w = 0, the rise time of μ_b was markedly shortened at T_w > 10 min, while its transient profile remained similar. In contrast, AI decreased substantially, and its variation depended on T_w.

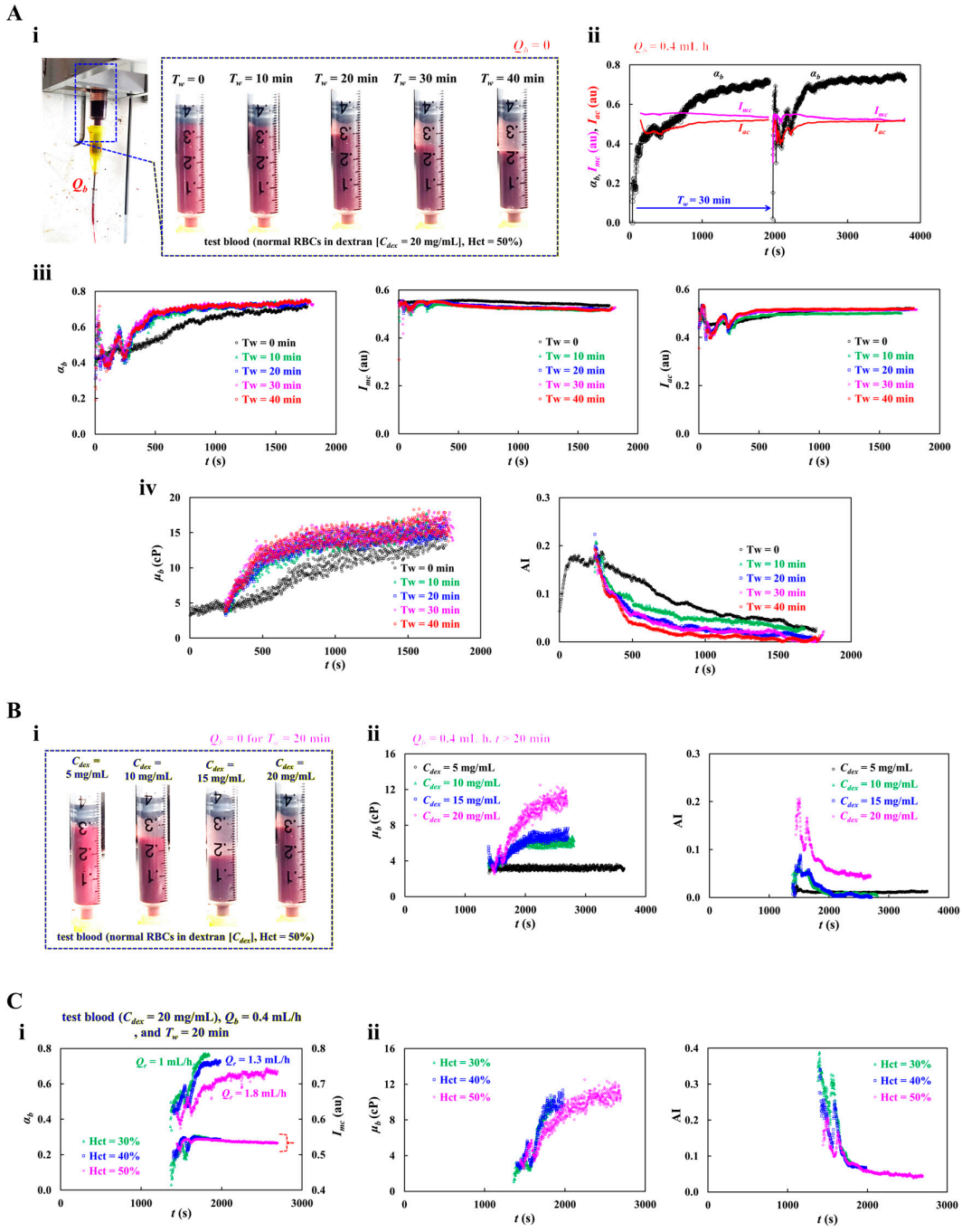

Figure 4. Quantitative evaluation of RBC sedimentation in a driving syringe using blood viscosity and RBC aggregation index. **(A)** Impact of no-delivery waiting time (T_w) to blood viscosity (μ_b) and RBC aggregation index

 doi:10.20944/preprints202603.2297.v1

(AI). Herein, test blood (Hct = 50%) was prepared by suspending normal RBCs into dextran solution (20 mg/mL). Flow-rate of blood was fixed at Q_b = 0.4 mL/h. **(i)** Snapshots showing RBC sedimentation with respect to no-delivery waiting time (T_w = 0 ~ 40 min). **(ii)** Timelapse α_b, I_{mc}, and I_{ac} with respect to T_w = 0, 30 min. Herein, flow rate of 1× PBS was set to Q_r = 1.8 mL/h. **(iii)** Timelapse α_b, I_{mc}, and I_{ac} with respect to T_w = 0 ~ 40 min. **(iv)** Timelapse μ_b and AI with respect to T_w. **(B)** Contribution of dextran solution to RBC sedimentation in a driving syringe. Herein, test blood (Hct = 50%) was prepared by suspending normal RBCs into dextran solution (C_{dex} = 5 ~ 20 mg/mL). **(i)** RBC sedimentation in a driving syringe as a function of C_{dex} after no-delivery waiting time of T_w = 20 min. **(ii)** Timelapse μ_b and AI with respect to C_{dex}. After an no-delivery waiting time of 20 min, blood was supplied at Q_b = 0.4 mL/h. **(C)** Contribution of hematocrit to RBC sedimentation in a driving syringe. No-delivery waiting time and blood flow-rate were set to T_w = 20 min and Q_b = 0.4 mL/h. **(i)** Timelapse Imc and αb with respect to Hct. **(ii)** Timelapse μ_b and AI with respect to Hct. .

Second, at T_w = 20 min, contribution of dextran solution to RBC sedimentation in a driving syringe was evaluated by measuring time-course of blood viscosity and RBC aggregation index. Herein, test blood (Hct = 50%) was prepared by suspending normal RBCs into dextran solution (C_{dex} = 5 ~ 20 mg/mL). As shown in Figure 4B-i, snapshots illustrating RBC sedimentation in the driving syringe were acquired as a function of C_{dex}. In general, higher dextran concentrations promoted faster RBC sedimentation[65,69]. Notably, however, sedimentation at C_{dex} = 20 mg/mL was much lower than that at C_{dex} = 15 mg/mL. After T_w = 20 min, flow rate of both fluids was set to Q_b = 0.4 mL/h and Q_r = 1.8 mL/h, respectively. Blood and 1× PBS were then supplied into each inlet of the microfluidic chip. **Figure 4B-ii** exhibited timelapse μ_b and AI with respect to C_{dex}. At C_{dex} = 5 mg/mL, both μ_b and AI remained nearly constant over time, indicating negligible RBC sedimentation in the syringe. For C_{dex} > 5 mg/mL, μ_b increased markedly as dextran concentration increased. It showed a significant upward trend over time. AI increased with respect to C_{dex}. However, it gradually decreased over time. Overall, the results demonstrated that RBC sedimentation strongly influenced both blood viscosity and AI.

Third, contribution of hematocrit to RBC sedimentation in a driving syringe was detected using time-course of blood viscosity and RBC aggregation index. Herein, test blood was prepared by suspending normal RBCs into dextran solution. No-delivery waiting time and blood flow-rate were set to T_w = 20 min and Q_b = 0.4 mL/h. **Figure 4C-i** showed timelapse I_{mc} and α_b with respect to Hct. Herein, the corresponding Q_r of each hematocrit was set to Q_r = 1 mL/h (Hct = 30%), Q_r = 1.3 mL/h (Hct = 40%), and Q_r = 1.8 mL/h (Hct = 50%). At Hct = 30% ~ 40%, the rising time of α_b was shortended when compared with Hct = 50%. The I_{mc} did not show substantial difference with respect to Hct. As shown in left-side panel of **Figure 4C-ii**, timelapse variations of μ_b were obtained with respect to Hct. The plateau level of μ_b remained comparable over the tested hematocrit range and showed no appreciable difference between Hct = 30% and 40%. In contrast, the rise time of μ_b was prolonged at Hct = 50%. As shown in right-side panel of **Figure 4C-ii**, timelapse AI were acquired with respect to Hct. The results showed that AI was initially higher at low hematocrit. However, after a certain time, hematocrit no longer had a significant effect on AI. In particular, at Hc = 30% ~ 40%, RBCs sedimentation was proceeded fast. Both μ_b and AI did not exhibit substantial difference with rspect to Hct = 30% or 40%.

The experiments showed that no-delivery waiting time strongly affected the time-dependent changes in blood viscosity and RBC aggregation index. Longer waiting times accelerated RBC sedimentation in the driving syringe, thereby altering both parameters over time. The suspending medium also had a significant effect on blood viscosity and RBC aggregation index. Therefore, to ensure consistent measurements, blood was loaded without a waiting period (T_w = 0).

3.4. Contribution of Blood Flow Condition in Quantification of Blood Properties

Previous studies commonly assessed the RBC aggregation index by abruptly stopping blood flow or shear[39,44,60,68,70]. In such on–off protocols, RBC aggregation was quantified under stationary blood, whereas blood viscosity was determined during the constant-flow phase[71].

 doi:10.20944/preprints202603.2297.v1

Because blood exhibits time-dependent transient rheology, viscosity values obtained immediately after flow switching may be less reliable than those measured after the flow reached a stable plateau at a defined shear condition[47,61]. Therefore, the conventional on–off flow method may be suboptimal for the simultaneous measurement of blood viscosity and RBC aggregation. In this section, based on time-course of blood viscosity and RBC aggregation index, the present continuous-flow method was quantitatively compared with the previous on–off method. Herein, test blood (Hct = 50%) was prepared by suspending normal RBCs into dextran solution (20 mg/mL). Flow rate of each fluid was set to Q_b = 0.4 mL/h and Q_r = 1.8 mL/h. In the previous method, the flow was controlled with T_{on}/T_{off} values of 2/2, 4/4, and 8/8 min/min.

As shown in **Figure 5A**, timelapse Q_{mc} and Q_{ac} were obtained with respect to T_{on}/T_{off} = 0, 2/2, 4/4, and 8/8 min/min. The steady plateau value of Q_{mc} was maintained at 0.4 mL/h. Under the constant flow-rate condition, Q_{mc} and Q_{ac} remained stable over time. In contrast, under the on–off flow condition, shorter switching periods did not provide a sufficiently long steady plateau in Q_{mc}. As the on–off period increased, the duration of the steady plateau also increased. Therefore, a longer on–off period, such as T_{on}/T_{off} = 8/8 min, was required to secure an adequately long plateau in the previous method. **Figure 5B** represented timelapse I_{mc}, I_{ac}, and α_b with respect to T_{on}/T_{off}. According to the results, under continuous blood flow, the time-dependent profiles of I_{mc}, I_{ac}, and α_b were obtained consistently and enabled appropriate analysis of blood changes. Under the on–off flow condition, however, α_b did not show a consistent trend because it included transient behavior. In contrast, the temporal variations of I_{mc} and I_{ac} were similar to those observed under continuous blood flow. **Figure 5C** presents the time-dependent variations in μ_b and AI with respect to T_{on}/T_{off}. The present method provided consistent temporal profiles of both parameters under continuous blood flow. Under the on–off flow condition, the overall profiles were similar to those obtained under continuous flow; however, because both μ_b and AI included transient responses, the previous method had limitations in the quantitative analysis of their time-dependent variations.

The experimental results confirmed that the present method was superior to the previous one. In particular, accurate monitoring of blood changes requires continuous measurement of blood viscosity and RBC aggregation index under continuous blood flow.

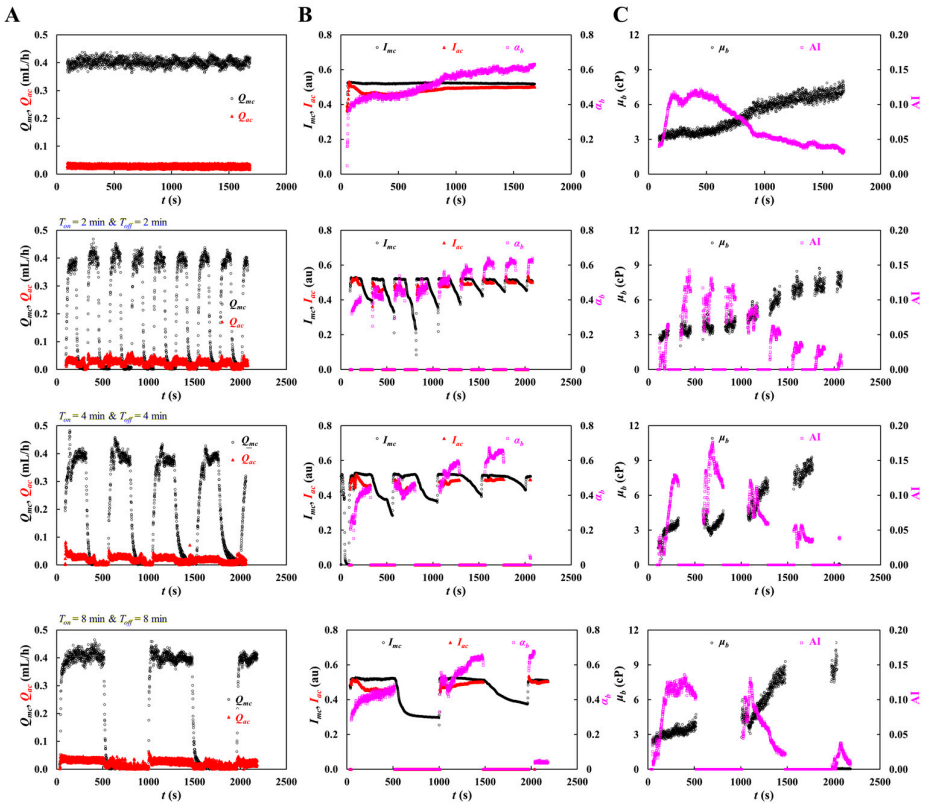

 doi:10.20944/preprints202603.2297.v1

Figure 5. Quantitative comparison between present method (continuous blood flow) and previous method (on-off blood flow) using blood viscosity and RBC aggregation. Herein, test blood (Hct = 50%) was prepared by suspending normal RBCs into dextran solution (20 mg/mL). Flow rate of each fluid was set to Q_b = 0.4 mL/h and Q_r = 1.8 mL/h. With regard to previous method, flow rate of both fluids was set to T_{on}/T_{off} = 2/2, 4/4, and 8/8 min/min. **(A)** Timelapse Q_{mc} and Q_{ac} with respect to T_{on}/T_{off}. **(B)** Timelapse I_{mc}, I_{ac}, and α_b with respect to T_{on}/T_{off}. **(C)** Timelapse μ_b and AI with respect to T_{on}/T_{off}. .

3.5. Quantitative Evaluation of Thermal-Exposed RBCs

At the last section, the present method was used to detect biophysical difference in thermal-exposed RBCs. Previous studies have shown that exposure of RBCs to elevated temperature significantly alters hemorheological properties, including blood viscosity, RBC aggregation, and deformability[72–75]. Herein, normal RBCs were incubated at 40 ~ 50 °C temperature for 20 min. Test blood (Hct = 50%) was then prepared by adding thermal-exposed RBCs into dextran solution (20 mg/mL). The corresponding flow rate of each was set to Q_b = 0.4 mL/h and Q_r = 1.8 mL/h.

First, contribution of heat-exposed temperature to blood viscosity (μ_b) and RBC aggregation index (AI) was quantitatively assessed. **Figure 6A-i** showed timelapse I_{mc}, I_{ac}, and α_b with respect to heat-shocked conditions (i.e., shocked-temperature = 40, 43, 45, and50 °C, and exposed time = 20 min). Notably, α_b showed little temporal variation under the high-temperature condition (50 °C for 20 min). Furthermore, the image intensity difference ($\Delta I = I_{mc} - I_{ac}$) progressively decreased with increasing incubation temperature of normal RBCs. As shown in **Figure 6A-ii**, timelapse μ_b and AI were obtained with respect to heat-exposed condition. The upper panel exhibited timelapse μ_b with respect to exposure temperature ranging from 40 °C to 50 °C. Initially, exposed time contributed to increasing μ_b substantially. When normal RBCs were incubated at 50 °C, test blood remained nearly constant over time. After an elapse of certain time, the μ_b was increased gradually over time. Timelapse μ_b did show slight difference with respect to exposed temperature. The lower panel presented the time-course of AI at different exposure temperatures. AI initially decreased substantially with increasing temperature. At 40 ~ 45 °C, it gradually decreased during blood delivery. However, it remained essentially unchanged at 50 °C. This indicated that RBC sedimentation was suppressed in the driving syringe after exposure to 50 °C, such that both μ_b and AI remained constant during continuous blood loading.

Second, based on experimental results, to assess contribution of heat-exposed time to blood viscosity and RBC aggregation index, heat-exposed temperature was set to 43 °C. The exposed time increased from 20 min to 165 min. **Figure 6B-i** presented timelapse I_{mc}, I_{ac}, and α_b with respect to heat-exposed condition. Based on timelapse I_{mc}, I_{ac}, and α_b, as shown in **Figure 6B-ii**, timelapse μ_b and AI were obtained with respect to exposed time. According to the results, μ_b increased gradually over time and showed no substantial dependence on exposure time. Similarly, the initial AI values did not differ markedly with exposure time. However, after a certain period, AI gradually decreased over time. Except for the 60 min exposure condition, the time-course of AI was independent of exposure time. Overall, incubation of normal RBCs at 43 °C for up to 120 min had no significant effect on the temporal variations of blood viscosity and RBC aggregation index.

Third, additionally, at the exposed temperature of 45 °C, incubation time increased from 20 min to 180 min. As shown in **Figure 6C-i**, timelapse I_{mc}, I_{ac}, and α_b were acquired with respect to heat-exposed time. The ΔI ($\Delta I = I_{mc} - I_{ac}$) declined at longer exposure times, whereas α_b was nearly constant over time except for the 20 min exposure. **Figure 6C-ii** exhibited timelapse μ_b and AI with respect to heat-exposed time. The upper panel presented time-course of μ_b at different exposure times. Compared with the control, μ_b of the test blood remained nearly constant over time and showed no substantial dependence on exposure time. The lower panel shows the time-course of AI at different exposure times. Compared with the control, AI of the test blood decreased markedly with increasing exposure time, but remained nearly constant over time. These results suggest that after incubation at 45 °C for more than 20 min, blood viscosity and AI stayed stable because thermally shocked RBCs no

 doi:10.20944/preprints202603.2297.v1

longer contributed to sedimentation in the driving syringe. Thermal-exposed time contributed to decreasing AI significantly.

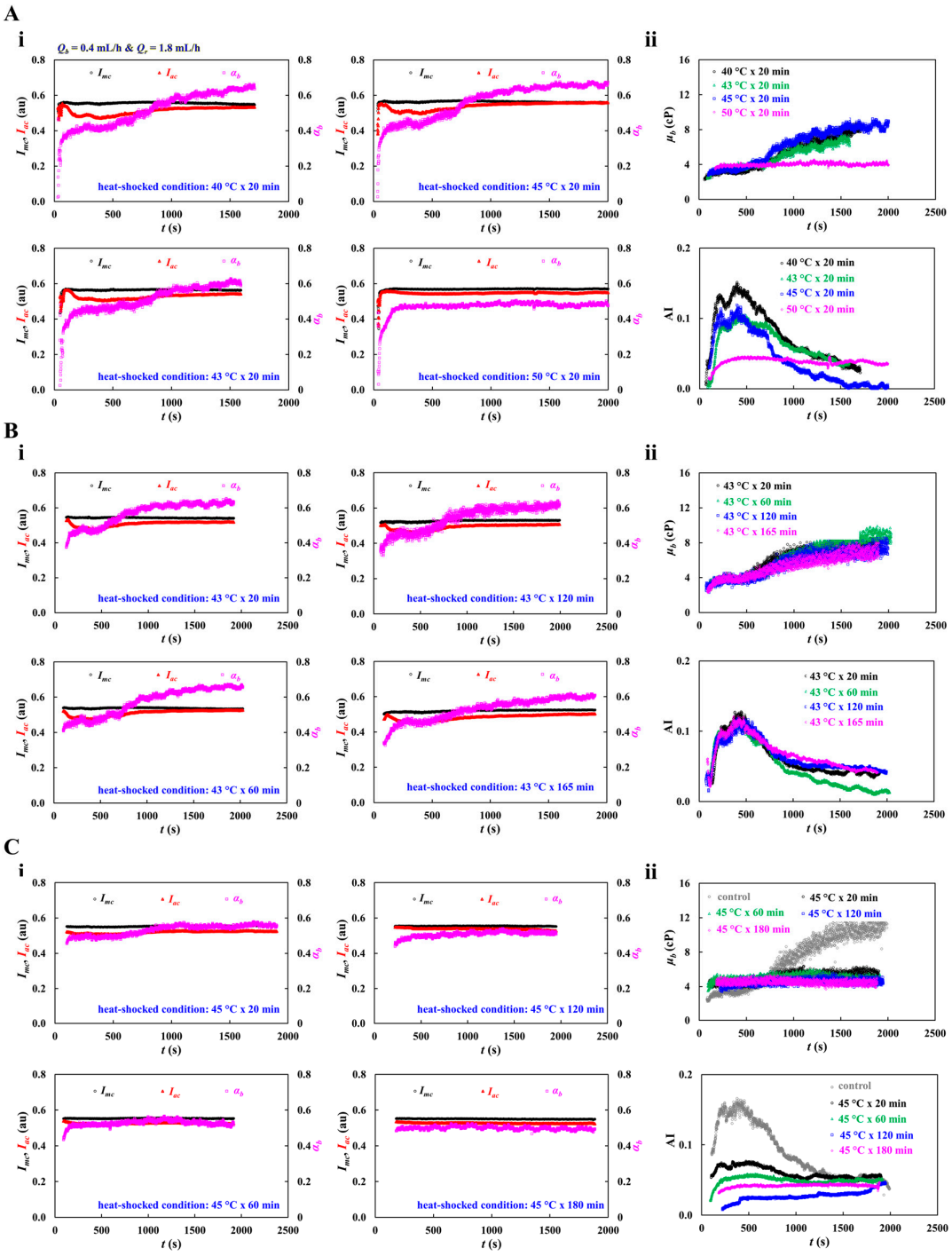

Figure 6. Quantitative evaluation of thermal-exposed RBCs using blood viscosity and RBC aggregation index. Herein, normal RBCs were incubated at 40 ~ 50 °C temperature for 20 min. Test blood (Hct = 50%) was then prepared by adding thermal-exposed RBCs into dextran solution (20 mg/mL). The corresponding flow rate of each was set to Q_b = 0.4 mL/h and Q_r = 1.8 mL/h. **(A)** Contribution of heat-exposed temperature to blood viscosity (μ_b) and RBC aggregation index (AI). **(i)** Timelapse I_{mc}, I_{ac}, and α_b with respect to heat-shocked condition (i.e., shock temperature = 40, 43, 45, and 50 °C, and exposed time = 20 min). **(ii)** Timelapse μ_b and AI with respect to heat-exposed condition. **(B)** Contribution of exposed time to blood viscosity and RBC aggregation index. Herein, normal RBCs were incubated at the temperature of 43 °C. The exposed time was set to 20, 60, 120, and 165 min.

 doi:10.20944/preprints202603.2297.v1

(i) Timelapse I_{mc}, I_{ac}, and α_b with respect to heat-exposed condition. **(ii)** Timelapse μ_b and AI with respect to heat-exposed condition. **(C)** Influence of incubation time to blood viscosity and RBC aggregation index. Herein, incubation time set to 20, 60, 120, and 180 min and exposed temperature set to 45 °C. **(i)** Timelapse I_{mc}, I_{ac}, and α_b with respect to heat-exposed time. **(ii)** Timelapse μ_b and AI with respect to heat-exposed time.

The experimental results lead to the conclusion that the proposed method could effectively detect hemorheological changes in thermal-shocked RBCs during continuous syringe delivery. Compared with control blood, heat-treated blood exhibited reduced AI and nearly constant time-course profiles of μ_b and AI, indicating that thermal shock suppressed RBC sedimentation and aggregation. At higher temperatures and longer exposure times, these effects became more evident, suggesting that heat-induced RBC damage minimized their contribution to sedimentation in the syringe. Therefore, the proposed method could be regarded as useful for assessing heat-induced alterations in RBC function.

4. Conclusions

This study proposed a microfluidic method for the simultaneous measurement of blood viscosity and RBC aggregation index under continuous blood delivery from a driving syringe. The results showed that both parameters were strongly affected by flow rate, hematocrit, suspension medium (dextran solution), and syringe on–off operation. In particular, flow interruption promoted RBC sedimentation in the syringe and consequently altered the measured hemorheological responses. These results highlighted the need to consider dynamic delivery conditions and demonstrated that the proposed method enabled reliable hemorheological analysis under continuous flow.

The method was further applied to characterize thermal-shock-induced changes in RBC behavior. Heat treatment reduced RBC aggregation and suppressed sedimentation, with these effects becoming more evident at higher temperatures and longer exposure times. Under severe thermal conditions, blood viscosity and aggregation index remained nearly constant over time, suggesting that thermally damaged RBCs no longer contributed substantially to sedimentation in the syringe. Therefore, the proposed method can serve as a sensitive and practical tool for simultaneous assessment of blood viscosity and RBC aggregation, as well as for detection of functional alterations in RBCs under continuous and non-interrupted blood flows. As a limitation, the proposed method was validated only with suspending blood. Thus, testing with patient blood samples will be required to verify its clinical applicability.

Author Contributions: Conceptualization, Y.J.K.; methodology, Y.J.K.; validation, Y.J.K.; formal analysis, Y.J.K.; investigation; data curation, Y.J.K.; writing—original draft preparation, Y.J.K.; writing—review and editing, Y.J.K.; visualization, Y.J.K.; supervision, Y.J.K.; project administration, Y.J.K.; funding acquisition, Y.J.K.

Funding: This study was supported by a research fund from the Chosun University in 2025.

Institutional Review Board Statement: This study was conducted in compliance with the Declaration of Helsinki and received approval from the Ethics Committee of Chosun University (reference code: 2-1041055-AB-N-01-2021-80).

Data Availability Statement: The original contributions presented in this study are included in the article material. Further inquiries can be directed to the corresponding author.

Acknowledgments: During the preparation of this manuscript/study, the author used ChatGPT (Ver. 5.4) for the purposes of generating text. The authors have reviewed and edited the output and take full responsibility for the content of this publication.

Conflicts of Interest: The authors declare no conflicts of interest.

 doi:10.20944/preprints202603.2297.v1

References

1. Cho, Y.I.; Cho, D.J. Hemorheology and microvascular disorders. Korean Circ. J. **2011,** 41, 287-95.
2. Piagnerelli, M.; Boudjeltia, K.Z.; Vanhaeverbeek, M.; Vincent, J.L. Red blood cell rheology in sepsis. Intensive Care Med. **2003,** 29, 1052-1061.
3. Rab, M.A.E.; Kanne, C.K.; Boisson, C.; Bos, J.; van Oirschot, B.A.; Houwing, M.E.; Renoux, C.; Bartels, M.; Rijneveld, A.W.; Nur, E.; Cnossen, M.H.; Joly, P.; Nader, E.; Fort, R.; Connes, P.; van Wijk, R.; Sheehan, V.A.; van Beers, E.J. Oxygen gradient ektacytometry-derived biomarkers are associated with acute complications in sickle cell disease. Blood Adv **2024,** 8, 276-286.
4. Mahawar, M.; Soni, B.; Nayak, A.K. An efficient approach for blood transport in complex interlinked micro-circulatory network. Physics of Fluids **2024,** 36, 121903.
5. Nader, E.; Skinner, S.; Romana, M.; Fort, R.; Lemonne, N.; Guillot, N.; Gauthier, A.; Antoine-Jonville, S.; Renoux, C.; Hardy-Dessources, M.D.; Stauffer, E.; Joly, P.; Bertrand, Y.; Connes, P. Blood rheology: key parameters, impact on blood flow, role in sickle cell disease and effects of exercise. Front Physiol **2019,** 10, 1329.
6. Woo, H.G.; Kim, H.G.; Lee, K.M.; Ha, S.H.; Jo, H.; Heo, S.H.; Chang, D.I.; Kim, B.J. Blood viscosity associated with stroke mechanism and early neurological deterioration in middle cerebral artery atherosclerosis. Sci. Rep. **2023,** 13, 9384.
7. Lu, M.; Rab, M.A.; Shevkoplyas, S.S.; Sheehan, V.A. Blood rheology biomarkers in sickle cell disease. Exp. Biol. Med. (Maywood) **2020,** 245, 155-165.
8. Kucukal, E.; Man, Y.; Hill, A.; Liu, S.; Bode, A.; An, R.; Kadambi, J.; Little, J.A.; Gurkan, U.A. Whole blood viscosity and red blood cell adhesion: Potential biomarkers for targeted and curative therapies in sickle cell disease. Am. J. Hematol. **2020,** 95, 1246-1256.
9. Choi, D.; Waksman, O.; Shaik, A.; Mar, P.; Chen, Q.; Cho, D.J.; Kim, H.; Smith, R.L.; Goonewardena, S.N.; Rosenson, R.S. Association of blood viscosity with mortality among patients hospitalized with COVID-19. J. Am. Coll. Cardiol. **2022,** 80, 316-328.
10. Baskurt, O.K.; Meiselman, H.J. Blood rheology and hemodynamics. Semin. Thromb. Hemost. **2003,** 29, 435-450.
11. Pajic-Lijakovic, I.; Milivojevic, M.; Barshtein, G.; Gural, A. The mechanical properties of erythrocytes are influenced by the conformational state of albumin. Cells **2025,** 14, 1139.
12. Caglar, S.E.; Karakoc, Y.; Tanoglu, A.; Demirtunc, R.; Tanrikulu, S.; Kilickaya, H.; Ercan, M. Investigation of hemorheology in patients with hyperthyroidism via blood viscosity, erythrocyte deformability and aggregation. Thyroid. Res. **2025,** 18, 11.
13. Gural, A.; Pajić-Lijaković, I.; Barshtein, G. Mechanical stimulation of red blood cells aging: focusing on the microfluidics application. Micromachines **2025,** 16, 259.
14. Gupta, S.; Wang, W.S.; Vanapalli, S.A. Microfluidic viscometers for shear rheology of complex fluids and biofluids. Biomicrofluidics **2016,** 10, 043402.
15. Del Giudice, F. A review of microfluidic devices for rheological characterisation. Micromachines (Basel) **2022,** 13, 167.
16. Kapadia, W.; V Giri, N.; Qin, N.; Zhao, P.; Phan, C.-M.; Haines, L.; Jones, L.; Ren, C.L. A novel microfluidic viscometer for measuring viscosity of ultrasmall volumes of Newtonian and non-Newtonian liquids. Journal of Micromechanics and Microengineering **2025,** 35, 055005.
17. Chen, W.; Xia, M.; Zhu, W.; Xu, Z.; Cai, B.; Shen, H. A bio-fabricated tesla valves and ultrasound waves-powered blood plasma viscometer. Front Bioeng Biotechnol **2024,** 12, 1394373.
18. Uno, M.O.; Omori, M.; Sakamoto, K. Nonwoven-fabric-based microfluidic devices for solution viscosity measurements. Sensors & Diagnostics **2024,** 3, 1551-1561.
19. Illibauer, J.; Clodi-Seitz, T.; Zoufaly, A.; Aberle, J.H.; Weninger, W.J.; Foedinger, M.; Elsayad, K. Diagnostic potential of blood plasma longitudinal viscosity measured using Brillouin light scattering. Proc Natl Acad Sci U S A **2024,** 121, e2323016121.
20. Chang, Y.N.; Yao, D.J. Development of a microfluidic viscometer for non-Newtonian blood analog fluid analysis. Bioengineering (Basel) **2024,** 11, 1298.

 doi:10.20944/preprints202603.2297.v1

21. Bakhtiaridoost, S.; Musuroi, C.; Volmer, M.; Florescu, M. Optoelectronic microfluidic device for point-of-care blood plasma viscosity measurement. Lab Chip **2024,** 24, 3305-3314.
22. Mustafa, A.; Haider, D.; Barua, A.; Tanyeri, M.; Erten, A.; Yalcin, O. Machine learning based microfluidic sensing device for viscosity measurements. Sensors & Diagnostics **2023,** 2, 1509-1520.
23. Gautam, N.; Ram, R.; Bishnoi, V.; Sarkar, A. A low-cost and disposable capillary-based paper sensor for measuring blood-plasma viscosity using a smartphone app. Microfluidics and Nanofluidics **2023,** 27, 41.
24. Trejo-Soto, C.; Lazaro, G.R.; Pagonabarraga, I.; Hernandez-Machado, A. Microfluidics approach to the mechanical Properties of Red Blood Cell Membrane and Their Effect on Blood Rheology. Membranes (Basel) **2022,** 12,
25. Trejo-Soto, C.; Hernandez-Machado, A. Normalization of blood viscosity according to the hematocrit and the shear rate. Micromachines (Basel) **2022,** 13, 357.
26. Kim, B.J.; Lee, Y.S.; Zhbanov, A.; Yang, S. A physiometer for simultaneous measurement of whole blood viscosity and its determinants: hematocrit and red blood cell deformability. Analyst **2019,** 144, 3144-3157.
27. Charansonney, O.L.; Meseguer, E.; Goube, P.; Vicaut, E. Erythrocyte aggregation kinetics for studying the vascular phase of inflammation in patients with suspected acute coronary syndrome or acute stroke. Sci Rep **2025,** 15, 38049.
28. Lee, C.A.; Farooqi, H.M.U.; Paeng, D.G. Axial shear rate: A hemorheological factor for erythrocyte aggregation under Womersley flow in an elastic vessel based on numerical simulation. Comput Biol Med **2023,** 157, 106767.
29. Puthumana Melepattu, M.; Maitrejean, G.; Wagner, C.; Podgorski, T. Influence of erythrocyte density on aggregability as a marker of cell age: Dissociation dynamics in extensional flow. J Biomech **2025,** 183, 112603.
30. Nam, J.H.; Xue, S.; Lim, H.; Shin, S. Study of erythrocyte aggregation at pulsatile flow conditions with backscattering analysis. Clin Hemorheol Microcirc **2012,** 50, 257-66.
31. Semenov, A.; Lugovtsov, A.; Ermolinskiy, P.; Lee, K.; Priezzhev, A. Problems of red blood cell aggregation and deformation assessed by laser tweezers, diffuse light scattering and laser diffractometry. Photonics **2022,** 9, 238.
32. You, J.; Park, C.-A.; Kim, A.-K.; Jeon, H.R.; Kim, D.-I.; Shin, S. Ultrasensitive microfluidic detection of red blood cell deformability: Age-related decline in deformability. Physics of Fluids **2025,** 37,
33. Liu, W.; Xie, L.; Yang, J.; Gong, X.; Sun, D.; Zhang, C. A microfluidic device for detecting the deformability of red blood cells. Biosensors (Basel) **2025,** 15, 758.
34. Kajitani, K.; Ohtani, T.; Higuchi, R.; Chimura, M.; Sera, F.; Tsai, C.D.; Ueda, Y.; Nishimura, J.I.; Sakata, Y. An on-chip deformability checker demonstrates that the severity of iron deficiency is associated with increased deformability of red blood cells. Sci Rep **2025,** 15, 19994.
35. Williams, D.C.; Wood, D.K. High-throughput quantification of red blood cell deformability and oxygen saturation to probe mechanisms of sickle cell disease. Proc Natl Acad Sci U S A **2023,** 120, e2313755120.
36. Kang, Y.J. A microfluidic-based blood viscometer. Physics of Fluids **2025,** 37, 091904.
37. Oh, K.W.; Lee, K.; Ahn, B.; Furlani, E.P. Design of pressure-driven microfluidic networks using electric circuit analogy. Lab Chip **2012,** 12, 515-45.
38. Alexandrova-Watanabe, A.; Abadjieva, E.; Ivanova, M.; Gartcheva, L.; Langari, A.; Guenova, M.; Tiankov, T.; Nikolova, E.V.; Krumova, S.; Todinova, S. Quantitative assessment of red blood cell disaggregation in chronic lymphocytic leukemia via software image flow analysis. Fluids **2025,** 10, 167.
39. Namgung, B.; Lee, T.; Tan, J.K.S.; Poh, D.K.H.; Park, S.; Chng, K.Z.; Agrawal, R.; Park, S.Y.; Leo, H.L.; Kim, S. Vibration motor-integrated low-cost, miniaturized system for rapid quantification of red blood cell aggregation. Lab Chip **2020,** 20, 3930-3937.
40. Kim, H.; Zhbanov, A.; Yang, S. Microfluidic systems for blood and blood cell characterization. Biosensors (Basel) **2022,** 13, 13.
41. Kang, Y.J. Microfluidic-based effective monitoring of bloods by measuring RBC aggregation and blood viscosity under stepwise varying shear rates. Korea-Aust. Rheol. J. **2020,** 32, 15-27.
42. Shin, S.; Yang, Y.; Suh, J.S. Measurement of erythrocyte aggregation in a microchip stirring system by light transmission. Clin Hemorheol Microcirc **2009,** 41, 197-207.

 doi:10.20944/preprints202603.2297.v1

43. Zhbanov, A.; Yang, S. Effects of Aggregation on Blood Sedimentation and Conductivity. PLoS One **2015,** 10, e0129337.
44. Baskurt, O.K.; Uyuklu, M.; Meiselman, H.J. Time course of electrical impedance during red blood cell aggregation in a glass tube: comparison with light transmittance. IEEE Trans Biomed Eng **2010,** 57, 969-78.
45. Kang, Y.J. Microfluidic-based technique for measuring RBC aggregation and blood viscosity in a continuous and simultaneous fashion. Micromachines (Basel) **2018,** 9, 467.
46. Antonova, N.; Khristov, K. Microrheological and microfluidic approaches for evaluation of the mechanical properties of blood cells. Applied Sciences **2025,** 15, 8291.
47. Kang, Y.J. Continuous and simultaneous measurement of the biophysical properties of blood in a microfluidic environment. Analyst **2016,** 141, 6583-6597.
48. Kang, Y.J. Assessment of continuous flow-dependent red cell aggregation using a microfluidic chip. Applied Sciences **2025,** 15, 11481.
49. Liang, M.; Ming, D.; Zhong, J.; Shannon, C.S.; Rojas-Carabali, W.; Agrawal, K.; Ai, Y.; Agrawal, R. Pathophysiological associations and measurement techniques of red blood cell deformability. Biosensors (Basel) **2025,** 15, 566.
50. Higuchi, M.; Watanabe, N. A rapid and accurate method for estimating the erythrocyte sedimentation rate using a hematocrit-corrected optical aggregation index. PLoS One **2022,** 17, e0270977.
51. Higuchi, M.; Watanabe, N. Determination of the erythrocyte sedimentation rate using the hematocrit-corrected aggregation index and mean corpuscular volume. J. Clin. Lab Anal. **2023,** 37, e24877.
52. Flormann, D.; Aouane, O.; Kaestner, L.; Ruloff, C.; Misbah, C.; Podgorski, T.; Wagner, C. The buckling instability of aggregating red blood cells. Sci Rep **2017,** 7, 7928.
53. Joo, J.B.; Kim, K.; Ro, W.B.; Lee, C.M. The erythrocyte sedimentation rate as a novel prognostic marker in canine inflammatory diseases. Animals (Basel) **2025,** 16, 40.
54. Kang, Y.J. Red blood cell sedimentation index using shear stress of blood flow in microfluidic channel. Biosensors (Basel) **2022,** 12, 547.
55. Kang, Y.J. Biomechanical investigation of red cell sedimentation using blood shear stress and blood flow image in a capillary chip. Micromachines (Basel) **2023,** 14, 1594.
56. Thielicke, W.; Stamhuis, E.J. PIVlab – towards user-friendly, affordable and accurate digital particle image velocimetry in MATLAB. Journal of Open Research Software **2014,** 2, e30.
57. Kloosterman, A.; Poelma, C.; Westerweel, J. Flow rate estimation in large depth-of-field micro-PIV. Experiments in Fluids **2010,** 50, 1587-1599.
58. Kim, G.; Jeong, S.; Kang, Y.J. Ultrasound standing wave-based cell-to-liquid separation for measuring viscosity and aggregation of blood sample. Sensors (Basel) **2020,** 20, 2284.
59. Guillot, P.; Panizza, P.; Salmon, J.-B.; Joanicot, M.; Colin, A. Viscosimeter on a microfluidic chip. Langmuir **2006,** 22, 6438-6445.
60. Kang, Y.J. Microfluidic chip for quantitatively assessing hemorheological parameters. Micromachines **2025,** 16, 567.
61. Kang, Y.J. Periodic and simultaneous quantification of blood viscosity and red blood cell aggregation using a microfluidic platform under in-vitro closed-loop circulation. Biomicrofluidics **2018,** 12, 024116.
62. Kang, Y.J. Microfluidic-based biosensor for blood viscosity and erythrocyte sedimentation rate using disposable fluid delivery system. Micromachines (Basel) **2020,** 11, 215.
63. Squires, T.M.; Mason, T.G. Fluid Mechanics of Microrheology. Annual Review of Fluid Mechanics **2010,** 42, 413-438.
64. Sebastian, B.; Dittrich, P.S. Microfluidics to Mimic Blood Flow in Health and Disease. Annual Review of Fluid Mechanics **2018,** 50, 483-504.
65. Bosek, M.; Ziomkowska, B.; Pyskir, J.; Wybranowski, T.; Pyskir, M.; Cyrankiewicz, M.; Napiorkowska, M.; Durmowicz, M.; Kruszewski, S. Relationship between red blood cell aggregation and dextran molecular mass. Sci. Rep. **2022,** 12, 19751.
66. Mehri, R.; Mavriplis, C.; Fenech, M. Red blood cell aggregates and their effect on non-Newtonian blood viscosity at low hematocrit in a two-fluid low shear rate microfluidic system. PLoS One **2018,** 13, e0199911.

 doi:10.20944/preprints202603.2297.v1

67. Brust, M.; Aouane, O.; Thiebaud, M.; Flormann, D.; Verdier, C.; Kaestner, L.; Laschke, M.W.; Selmi, H.; Benyoussef, A.; Podgorski, T.; Coupier, G.; Misbah, C.; Wagner, C. The plasma protein fibrinogen stabilizes clusters of red blood cells in microcapillary flows. Sci. Rep. **2014,** 4, 4348.
68. Shin, S.; Nam, J.H.; Hou, J.X.; Suh, J.S. A transient, microfluidic approach to the investigation of erythrocyte aggregation: the threshold shear-stress for erythrocyte disaggregation. Clin Hemorheol Microcirc **2009,** 42, 117-25.
69. Zhang, Z.W.; Neu, B. Role of macromolecular depletion in red blood cell adhesion. Biophys. J. **2009,** 97, 1031-1037.
70. Dobbe, J.G.; Streekstra, G.J.; Strackee, J.; Rutten, M.C.; Stijnen, J.M.; Grimbergen, C.A. Syllectometry: the effect of aggregometer geometry in the assessment of red blood cell shape recovery and aggregation. IEEE Trans. Biomed. Eng. **2003,** 50, 97-106.
71. Valerio de Arruda, M.; Cruz Silva, A.; Fernandes Galduroz, J.C.; Ferreira Galduroz, R. Standardization for obtaining blood viscosity: A systematic review. Eur J Haematol **2021,** 106, 597-605.
72. Buono, M.J.; Krippes, T.; Kolkhorst, F.W.; Williams, A.T.; Cabrales, P. Increases in core temperature counterbalance effects of haemoconcentration on blood viscosity during prolonged exercise in the heat. Exp. Physiol. **2016,** 101, 332-342.
73. Matrai, A.A.; Varga, G.; Tanczos, B.; Barath, B.; Varga, A.; Horvath, L.; Bereczky, Z.; Deak, A.; Nemeth, N. In vitro effects of temperature on red blood cell deformability and membrane stability in human and various vertebrate species. Clin Hemorheol Microcirc **2021,** 78, 291-300.
74. Cha, S.; Shin, T.; Lee, S.S.; Shim, W.; Lee, G.; Lee, S.J.; Kim, Y.; Kim, J.M. Cell stretching measurement utilizing viscoelastic particle focusing. Anal. Chem. **2012,** 84, 10471-10477.
75. Lee, S.S.; Yim, Y.; Ahn, K.H.; Lee, S.J. Extensional flow-based assessment of red blood cell deformability using hyperbolic converging microchannel. Biomed. Microdevices **2009,** 11, 1021-1027.